

# Adjustment of the Seismic Collapse Fragility Curves of Structures by Considering the Ground Motion Spectral Shape Effects

ALIREZA AZARBAKHT<sup>1</sup>, MEHDI MOUSAVI<sup>1</sup>, and MOHSEN GHAFORY-ASHTIANY<sup>2</sup>

5

<sup>1</sup>Department of Civil Engineering, Arak University, Iran

<sup>2</sup>International Institute of Earthquake Engineering and Seismology, (IIEES), Tehran, Iran

*The influence of the indicator  $\eta$  on the collapse capacity of structural systems has been investigated in this article. Eta has been introduced recently as an indicator of spectral shape which has strong influence on the structural nonlinear response. In this article, a closed form formula has also been developed to predict the collapse capacity of structures as a function of their structural behaviour parameters. The collapse fragility of a given structure can be determined for different hazard levels by adjusting the single fragility which results from a general set of ground motion records. The results of a seismic collapse risk analyses of a four- and an eight-story reinforced concrete test structure have confirmed the consistency of the proposed simple approach which is valid for period range of 0.25–3.0 s and the ductility range of 4–12.*

10

15

**Keywords** Collapse Capacity; Seismic Fragility Curve; Spectral Shape; Epsilon; Eta

## 1. Introduction

The mean annual frequency (MAF) of the seismic collapse can be calculated, for a given structure, by integrating the collapse fragility curve over the site hazard curve [McGuire, 1995]. Calculation of the hazard curve for a given site is a straightforward procedure, but the collapse fragility assessment process has not yet been thoroughly implemented. The most important challenge for the seismic collapse assessment of structures is the lack of reliable analytical models. Adequate structural models do not yet exist, which could capture the complex phenomena which result in collapse, such as cascading (progressive) collapse or the loss of vertical load-carrying capacity in individual structural elements [Zareian and Krawinkler, 2007]. The most practical limit state of collapse is dynamic instability in one or more stories of the structural model [Ibarra and Krawinkler, 2005]. This dynamic instability is due to the deterioration of the structural elements and/or P- $\Delta$  effects.

20

25

30

Another challenge in seismic collapse fragility assessment is to select a suitable set of ground motion records. From the seismological point of view, the selected ground motion records should represent the magnitude and distance identified by probabilistic seismic hazard analysis (PSHA) disaggregation [Bazzurro and Cornell, 1999]. It has been shown

Received 12 June 2011; accepted 11 June 2012.

Address correspondence to Alireza Azarbakht, Department of Civil Engineering, Faculty of Engineering, Arak University, Iran, P.O. Box 38156-88359. E-mail: a-azarbakht@araku.ac.ir

that the selection of ground motion records based only on the consistency of the magnitude and distance, without any constraints on the scaling limits, causes the occurrence of bias and dispersion in the nonlinear response of structures [Luco and Bazzurro, 2007]. For better clarification, assume two ground motion records both of which meet the magnitude and distance criteria for a considered site. Also assume that the response spectrum of the first record is close to that predicted by a standard attenuation relationship, whereas the response spectrum of the second record is quite extreme (rare). By scaling these records to a characteristic level of intensity, it has been shown that the spectral shapes of the records are completely different [Baker and Cornell, 2006]. Consequently, the structural nonlinear response for these records, too, can be expected to differ very significantly. Consistent with this trend, the appropriate records for a desired level of hazard are those which need a minimum level of scaling. This is the main idea of the  $\varepsilon$ -filtration approach, which was proposed by Baker and Cornell [2006]. The parameter  $\varepsilon$  was defined as a measure of the difference between the spectral acceleration of a record and the mean value obtained from a ground motion prediction equation for a given period. Despite its simplicity, it has been shown that the parameter  $\varepsilon$  is an indicator of the spectral shape and thus also a predictor of the nonlinear response of a structure. As a direct approach for the consideration of the spectral shape in the record selection, a target  $\varepsilon$  value, associated with a selected hazard level, is first obtained from the hazard disaggregation procedure, and then records with a closer  $\varepsilon$ -value to the target value can be chosen.

Recently, a more robust predictor of spectral shape was proposed by the authors [Mousavi *et al.*]. The new parameter, which has been named  $\eta$ , is a linear combination of the response spectra epsilon ( $\varepsilon_{Sa}$ ) and the peak ground velocity epsilon ( $\varepsilon_{PGV}$ ). A brief background for this parameter is presented in the following section. Q2

The major challenge in considering the spectral shape for the selection of records (via  $\varepsilon$  or  $\eta$ -filtration) lies in the finding of different sets of ground motion records for each level of hazard for calculation of the MAF of a limit-state for a given structure. Due to the dependence of  $\varepsilon$  or  $\eta$  on period, it may not be practical to select different specific ground motion sets for any specified period ( $T_1$ ) corresponding to a given site with a particular hazard level. Recently, a simple approach was proposed by Haselton *et al.* [2011], which could be used instead of the direct selection approach. In this solution, whose use was proposed in the ATC63 project [FEMA, 2009], it is suggested that a general set of ground motion records could be used for assessment of the collapse fragility of any structure, without considering the spectral shape of the records. The resulting mean collapse capacity can then be adjusted to meet the hazard-related target  $\varepsilon$  value.

The aim of this article is to propose a simple approach for adjustment of the seismic collapse fragility of a given structure to different hazard levels through a consideration of the parameter  $\eta$  as an indicator of spectral shape. Due to the greater strength of  $\eta$  as an indicator of spectral shape, in comparison with the parameter  $\varepsilon$ , it was anticipated that adjustment of the collapse fragility curve of a structure based on this parameter could lead to more reliable MAF results. It should be noted that since the application domain of the  $\eta$ -filtration approach is limited to the periods from 0.25–3.0 s, the application of the proposed procedure should be constrained to this range of period, as well as the ductility range of 4–12.

## 2. Eta; A New Indicator of Elastic Spectral Shape

$\varepsilon$  is a general notation for the spectral response epsilon, and can be given the more meaningful notation  $\varepsilon_{Sa}$ . The initial form of  $\eta$  has been defined as [Mousavi *et al.*, ]:

$$\eta = \varepsilon_{Sa} - 0.823\varepsilon_{PGV}, \quad (1)$$

where  $\varepsilon_{PGV}$  is the peak ground velocity (PGV) epsilon. Both  $\varepsilon_{Sa}$  and  $\varepsilon_{PGV}$  can be calculated from an attenuation relationship. It is worth emphasizing that the older attenuation relationships, such as AS97 [Abrahamson and Silva, 1997] or BJK [Boore *et al.*, 1997], are not able to predict the PGV, so it is necessary to refer to the newer attenuation models such as CB07 [Campbell *et al.*, 2007]. In all parts of this article, CB08 has been used as an appropriate ground motion prediction model.

To explain the effectiveness of  $\eta$  as an indicator of spectral shape, a set of 78 records with a magnitude range of 6.5–7.8 was selected [PEER, ]. The selection criteria and the other information of this set can be found in Haselton and Deierlein [2007]. First, the mentioned records have been scaled to  $S_a(T=1.0\text{ s}) = 1.0$ . They were then sorted based on their  $\varepsilon$  and  $\eta$  values. Finally, two higher and lower subsets with  $N$  elements were selected from each sorted list. The mean of the response spectra of each of the subsets was plotted in Fig. 1, in which the left-hand figures are based on  $\varepsilon$  sorting, and the right-hand figures on  $\eta$  sorting. The two subsets, each containing eight records, as shown in Fig. 1a, result in different spectral shapes. This difference in the spectral shape of the records with positive and negative  $\varepsilon$  was expected according to the results of other studies [e.g., Baker and Cornell, 2006]. The procedure is repeated for  $\eta$ -filtration in Fig. 1b. The difference between two resulting spectra is more significant in the case of  $\eta$ -filtration than in the case of  $\varepsilon$ -filtration. This analysis was repeated for a subset of 16 records, and the corresponding results are shown in Figs. 1c and d, for both filtration approaches. The obtained results

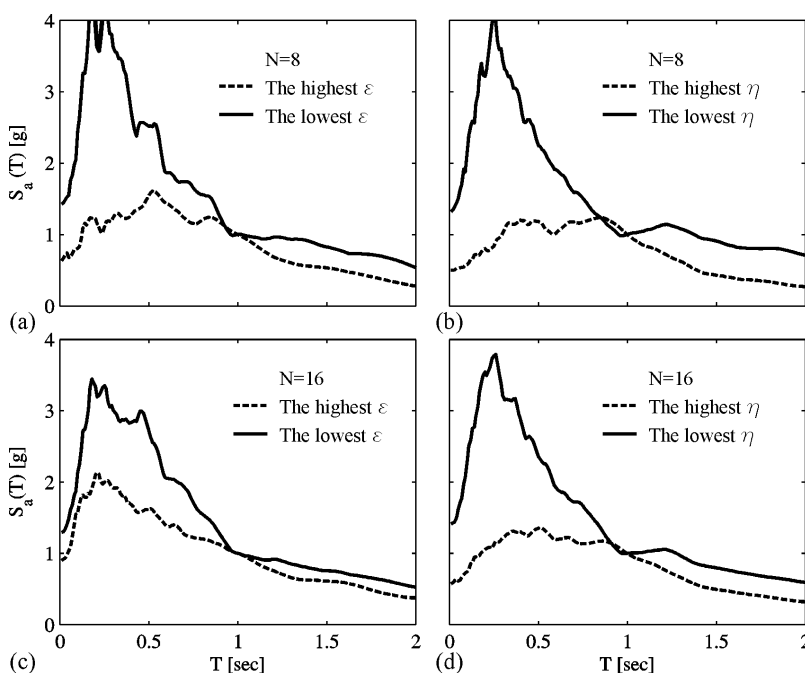


**FIGURE 1** Comparison of  $\eta$  and  $\varepsilon$  as indicators of spectral shape [7]. (a), (b) Selection of 8 records with highest/lowest values of  $\varepsilon$  and  $\eta$ ; (c), (d) Selection of 16 records with highest/lowest values of  $\varepsilon$  and  $\eta$ .

confirm the greater robustness of  $\eta$  as a parameter for distinguishing between records with different spectral shapes.

A practical challenge faced when using  $\eta$  for record selection is the choice of the target  $\eta$ . Ground-motion prediction models predict the probability distributions of intensity measures for a specified earthquake event. These models provide only marginal distributions, but they do not specify correlations among differing intensity measures. On the other hand, standard hazard disaggregation analysis only provides the target  $\varepsilon_{Sa}$ , but the target  $\varepsilon_{PGV}$  is still undetermined. The correlation between  $\varepsilon_{PGV}$  and  $\varepsilon_{Sa}$  in different period ranges has been studied [Mousavi *et al.*, ], and an analytical equation has been proposed for the evaluation of  $\varepsilon_{PGV}$  for a given  $\varepsilon_{Sa}$ :

$$\varepsilon_{PGV} = 0.21 + 0.77\varepsilon_{Sa}. \quad (2)$$

The validation of this equation has been illustrated for the period range 0.25–3.0 s. The direct method to account for the  $\eta$  in response assessment is to determine the expected  $\varepsilon_{PGV}$  value from Eq. (2) for any considered hazard level, then, to calculate the target  $\eta$  from Eq. (1), and finally, to select the ground motions that are consistent with the target  $\eta$ . For the purposes of simplicity, Eq. (1) has been revised to normalize the target  $\eta$  values to the target  $\varepsilon_{Sa}$  values, as described below:

$$\eta = k_0 + k_1(\varepsilon_{Sa} - b\varepsilon_{PGV}). \quad (3)$$

It is clear that, due to the linear correlation between  $\eta$  values and the structural response, this adjustment is permissible. Now, by substituting  $\varepsilon_{PGV}$  from Eq. (2) into Eq. (3), and considering the target  $\eta$  to be equal to the target  $\varepsilon_{Sa}$ ,  $k_0, k_1$  can be determined as:

$$k_0 = \frac{bc_0}{1 - bc_1} = 0.472, \quad k_1 = \frac{1}{1 - bc_1} = 2.730.$$

By replacing the above constant values in Eq. (3), the final form of  $\eta$  is obtained as:

$$\eta = 0.472 + 2.730\varepsilon_{Sa} - 2.247\varepsilon_{PGV}. \quad (4)$$

The target  $\eta$  value can now be considered to be equal to the target  $\varepsilon_{Sa}$  which can usually be obtained from seismic disaggregation analysis. Then the records can be filtered based on the difference between the target  $\eta$  and each record's  $\eta$  which is calculated based on Eq. (4).

### 3. Sensitivity of Collapse Fragility Curves to Eta Value

The collapse capacity for a distinct ground motion record is obtained by performing incremental dynamic analysis (IDA) [Vamvatsikos and Cornell, 2002], in which the intensity measure (IM) of that ground motion is increased and nonlinear response history analysis is performed until the dynamic instability is occurred. The precise trace of the collapse point was done using the Hunt and Fill algorithm [Vamvatsikos and Cornell, 2002]. By assuming a lognormal distribution for the resulted IMs, the collapse fragility curve is achievable.

The sensitivity of collapse fragility curves to both of  $\varepsilon$  and  $\eta$  values has been studied in this section by employing a single-degree-of-freedom (SDOF) system. This simple oscillator uses a moderately pinching hysteresis model with no cyclic deterioration, developed by Ibarra and Krawinkler [2005], having  $\xi=5\%$  viscous damping and  $T_1=1.0$  s period. Also,

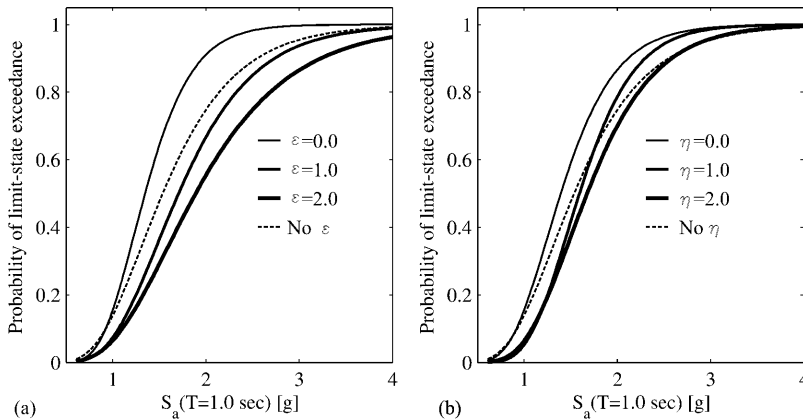


**FIGURE 2** The influence of the consideration of spectral shape on the fragility assessment of a SDOF system with  $T=1.0$  s, and  $\mu=8$ . (a)  $\varepsilon$ -filtration and (b)  $\eta$ -filtration.

an elastic-perfectly-plastic backbone curve is engaged for this system and P- $\Delta$  effects were neglected, for the purpose of simplicity. The collapse capacity for this structure is defined as the ratio of the collapse spectral acceleration to the yield level of spectral acceleration. This collapse capacity is noted as  $R$  in this article. 140

From the ground motion set cited in the former section, six subsets were chosen and the associated collapse fragility curves for these sets are shown in Fig. 2. The criterion for selection of these subsets is the specified  $\varepsilon$  and  $\eta$  values at period  $T=1.0$  s, representing different hazard levels. The collapse fragility related to all of the records (without any filtration) is also plotted for comparison. 145

The fact that consideration of  $\varepsilon$  and  $\eta$  significantly affects the seismic fragility curves is demonstrated in Fig. 2. It can be seen that, in the case of lower probability hazard levels (rare events), the median collapse capacity obtained by ignoring the effects of  $\varepsilon$  and  $\eta$  is underestimated, but vice versa for higher probability hazard levels. Another finding is that the different filtration approaches may lead to a different collapse capacity median and different dispersion. It is clear that the dispersion in the response corresponding to the  $\varepsilon$ -filtration approach is comparable to the dispersion obtained without filtration, but  $\eta$ -filtration leads to less dispersion in the response. 150

Due to the significant effect of spectral shape on the collapse fragility curves, this filtration is a logical strategy for risk-analysis objectives. However, since consideration of the spectral shape (via  $\varepsilon$  or  $\eta$ -filtration) for calculating the MAF of collapse necessitates repetition of the filtration for each step of the integration (for different hazard levels), the practicality of this approach is questionable. Considering the spectral shape in the structural collapse fragility assessment without the need to select a unique set of ground motions is a sensible idea. 155 160

#### 4. Adjustment of Fragility Curve Through Use of Eta

The adjustment of fragility curve to different spectral shape was originally introduced by Haselton *et al.* [2011]. Different multi-degree-of-freedom (MDOF) systems were used in the mentioned work to investigate the impact of  $\varepsilon$  on the shifting the general fragility curve. Finally, a closed form formula was proposed to quantify the influence of structural parameters on the rate of this shifting. This work is repeated again in this paper, except that 165

the adjustment is done through the parameter  $\eta$  as a more robust indicator of the spectral shape. Furthermore, simple SDOF systems are used here to develop the adjustment formula instead of the complex MDOF systems.

Similar to Haselton *et al.* [2011], the adjustment procedure can be depicted with a simple example. Assume two SDOF systems with period values equal to 0.5 and 1.5 s, the limit-state ductility values equal to 4 and 12, and other structural parameters similar to that introduced in the former section. The relationship between  $\eta$  and the logarithm of the collapse capacity (R) is shown in Fig. 3, from which it can be seen that the nonlinear response can be predicted as a function of  $\eta$ .

It is interesting to highlight the coefficient of correlation between LN(R) and  $\eta$  in Fig. 3 which is 0.63 for first SDOF, and 0.75 for the other one. If this analysis is repeated for  $\varepsilon$ , the resulted coefficients of correlation are 0.43 and 0.57, respectively. The more strength correlation between the structural response and  $\eta$  is another evidence for this claim that  $\eta$  is more reliable response predictor, comparing with  $\varepsilon$ .

As a consequence of the linear relationship between LN(R) and  $\eta$ , if the collapse capacity of a structure is available based on a general set of records, the response of that structure at different hazard levels can be evaluated with a closed form function, instead of by a particular selection of records for each hazard level.

Consider a linear model for the prediction of the collapse capacity as a function of  $\eta$ :

$$LN(R) = \alpha + \beta\eta, \quad (5)$$

where  $\alpha$  and  $\beta$  are constant values. If a general set of records results in a mean log collapse capacity equal to  $\bar{m}$ , then the target mean log collapse capacity ( $m^*$ ) for a specific hazard level ( $\eta^*$ ) can be calculated as:

$$m^* = \bar{m} + \beta (\eta^* - \bar{\eta}), \quad (6)$$

where  $\bar{\eta}$  is the mean value of  $\eta$  for the general records corresponding to the characteristic period of the structure. Thus,  $\beta$  is the basic parameter for the adjustment of the response to

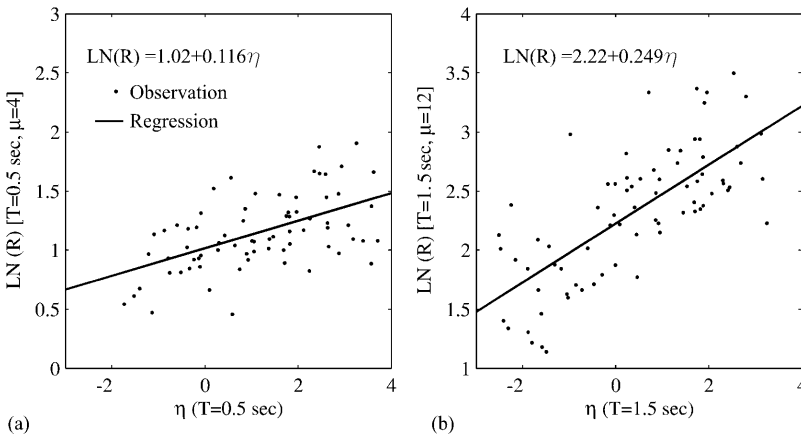


**FIGURE 3** Prediction of the limit-state capacity of SDOF systems as a function of  $\eta$ . (a)  $T=0.5$  s,  $\mu=4$  and (b)  $T=1.5$  s,  $\mu=12$ .

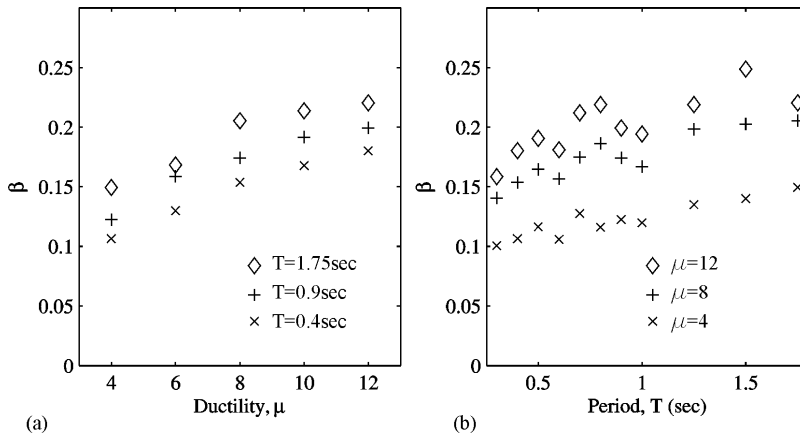


**FIGURE 4**  $\beta$  plotted as a function of ductility and period. (a) Variation of  $\beta$  with ductility and (b) variation of  $\beta$  with period.

different hazard levels. As shown in Fig. 4, the value of  $\beta$  varies for structures with different behaviour parameters i.e., period and ductility.

As can be seen from Fig. 4, the variation of  $\beta$  vs. period and ductility is significant, and can be analyzed as a meaningful phenomenon. The parameter  $\beta$  is similar to the parameter  $\beta_1$  which was introduced by Haselton *et al.* [2011] to adjust the mean collapse capacity through the use of the parameter  $\varepsilon$ . They analyzed  $\beta_1$  as a function of two key structural parameters: the number of stories of the building ( $N$ ), and the ultimate roof drift ratio at a strength loss of 20% (RDR). The current study is based on the use of SDOF systems in order to analyze the effect of structural parameters on the value of  $\beta$ . It is obvious that a complex system cannot satisfactorily be identified by a few features, i.e.,  $N$  and RDR. A complex system defined by  $N$  and RDR may not have a significant advantage related to a simple elastic-perfectly-plastic system characterized by  $T$  and final  $\mu$ . In addition to that, using the equivalent SDOF system to predict the dynamic behavior of a complex MDOF is also utilised as an efficient approach in many other research works (e.g., Vamvatsikos and Cornell, 2005; Azarbakht and Dolšek, 2011). The variable parameters of SDOF model are period and ductility.

Finding a closed form which could be used to predict  $\beta$  as a function of the period and the ductility is the goal of the next section.

#### 4.1. Regression of the Parameter $B$ Using Genetic Programming

The Genetic Programming (GP) is a symbolic optimization technique which can solve a problem using the principle of Darwinian natural selection. The symbolic optimization algorithms present the potential solutions by the structural ordering of several symbols. Interested readers can find more details about GP in Banzhaf *et al.* [1998].

The combination of 11 period values ( $T=0.3, 0.4, 0.5, 0.6, 0.7, 0.8, 0.9, 1.0, 1.25, 1.5,$  and  $1.75$  s) and 5 ductility values ( $\mu=4, 6, 8, 10,$  and  $12$ ) creates 55 SDOF models for the GP analysis. The other structural parameters are similar to that introduced in Sec. 2. The SDOF data set was randomly divided into training and testing subsets. In order to achieve consistent data division, several combinations of the training and testing sets were considered. The selection was such that the maximum, minimum, mean, and standard deviations of the parameters were consistent in the training and testing data sets. Out of the

55 items of data, 44 items (80%) were used as training data, and 11 items (20%) were used for testing of the generalization capability of the models.

In order to obtain a simple and straightforward formula, four basic arithmetic operators (+, −, ×, /) were used in the analysis. In order that the best results be obtained by the GP algorithm, the parameter  $\beta$  was defined as in Eq. (7):

225

$$\beta = c_0 - \frac{c_1}{(T + c_2)(\mu + c_2)}$$

$$c_0 = 0.259, \quad c_1 = 2.15, \quad c_2 = 1.81. \quad (7)$$

Based on the logical hypothesis [Smith, 1986] that, if a model achieves a correlation coefficient of more than 80%, and if the error values (e.g., the root mean square error, RMSE) are at their minimum, there is a strong correlation between the predicted and observed values. It can be seen in Fig. 5 that the proposed GP model with a high  $\rho$  and low RMSE values is able to predict the target values with an acceptable degree of accuracy. It should also be noted that the RMSE value is not only low, but also very similar to the values corresponding to the training and testing sets, which suggests that the proposed model has sufficient prediction capability.

230

The predicted trend of  $\beta$  vs. period and ductility, as well as the observed data points in a few samples, is shown in Fig. 6, whereas the ratio of the observed value of  $\beta$  to the predicted value is shown vs. the ductility and period values in Fig. 7. It can be seen from the latter that this ratio falls within the range from 0.8–1.2 for all of the SDOF systems, which is smaller than range from 0.5–1.5 which was the case in Haselton *et al.* [2011]. It seems that this range of error may have a significant effect on the assessed structural response and consequently on MAF calculations. A comprehensive analysis of uncertainty propagation is needed to study this hypothesis which is open for future researches.

235

240

The mean collapse capacity for a target hazard level can be achieved through calculation of  $\beta$  from Eq. (7), and then adjustment of the general mean collapse capacity to that hazard level can be performed by using Eq. (6). The only remaining parameter for adjustment of collapse fragility for a desired hazard level is the dispersion of the response, which is discussed in the following section.

245

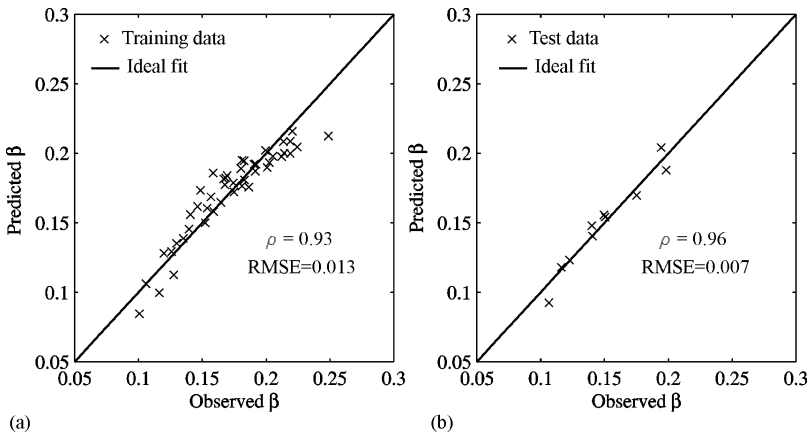


**FIGURE 5** Predicted vs. observed  $\beta$  values using the GP model. (a) Training data and (b) test data.

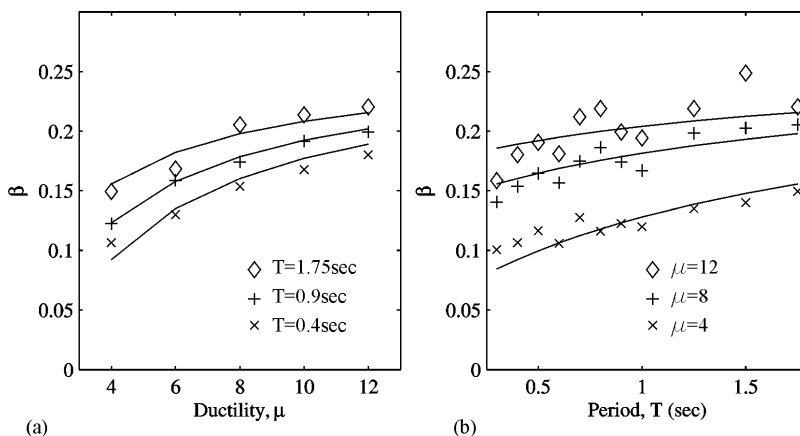


**FIGURE 6** The predicted trend of  $\beta$  as a function of ductility and period. (a) Prediction of  $\beta$  as a function of ductility and (b) prediction of  $\beta$  as a function of period.

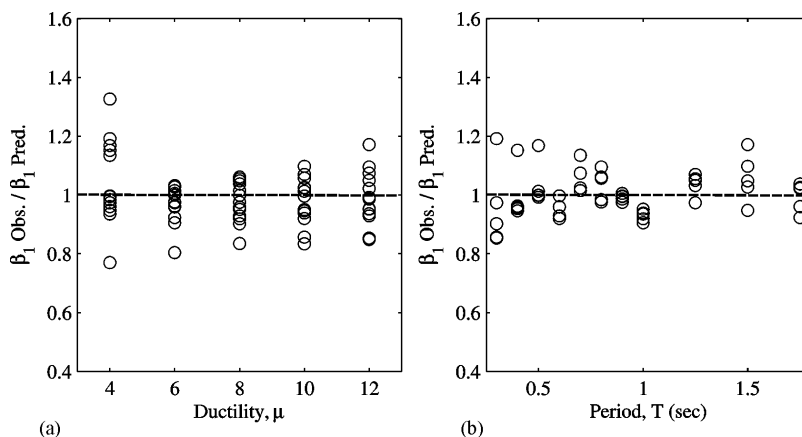


**FIGURE 7** Ratio of the observed values of  $\beta$  to the predicted values, plotted against (a) ductility and (b) period.

**4.2. Reduction in the Dispersion of the Structural Response**

As shown in Fig. 2, consideration of  $\eta$  leads to a clear reduction in the dispersion of structural collapse capacity, contrary to the almost negligible reduction which resulted from  $\varepsilon$ -filtration. 250

Figure 8 shows the dispersion of collapse capacity for two SDOF systems, based on a selection of 20 records for different levels of  $\varepsilon$  and  $\eta$ . Also, for comparison, the dispersion of response for the “no filtration case” has been included. The reduction in dispersion for both of the filtration approaches can be seen in Fig. 8, and it can also be seen that the  $\eta$ -filtration approach leads to a greater reduction in dispersion than the  $\varepsilon$ -filtration approach. 255  
 Recall that x-axis shows the target  $\varepsilon$  that is identical to the target  $\eta$ . In order to verify the significance of this trend, the fractional reduction in dispersion is shown in Fig. 9 for a wide range of SDOF systems, for both filtration approaches. The average reduction in dispersion amounts to 10% and 25%, respectively, for  $\varepsilon$  and  $\eta$ -filtration.

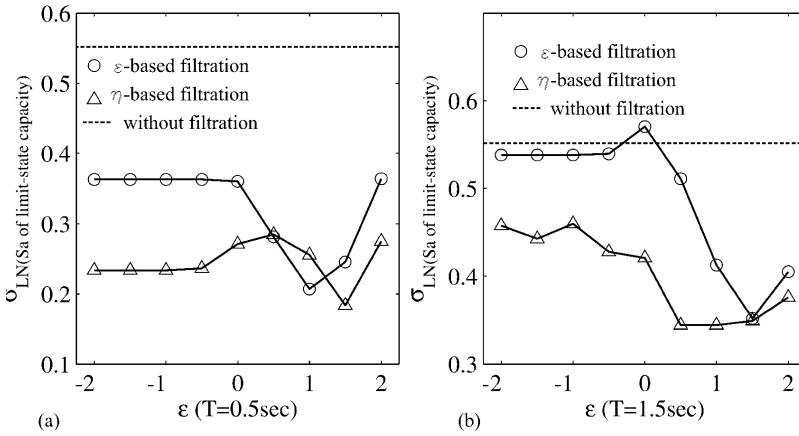


**FIGURE 8** Dispersion of SDOF limit-state capacity for the two different selection approaches. (a)  $T=0.5$  s,  $\mu=4$  and (b)  $T=1.5$  s,  $\mu=12$ .

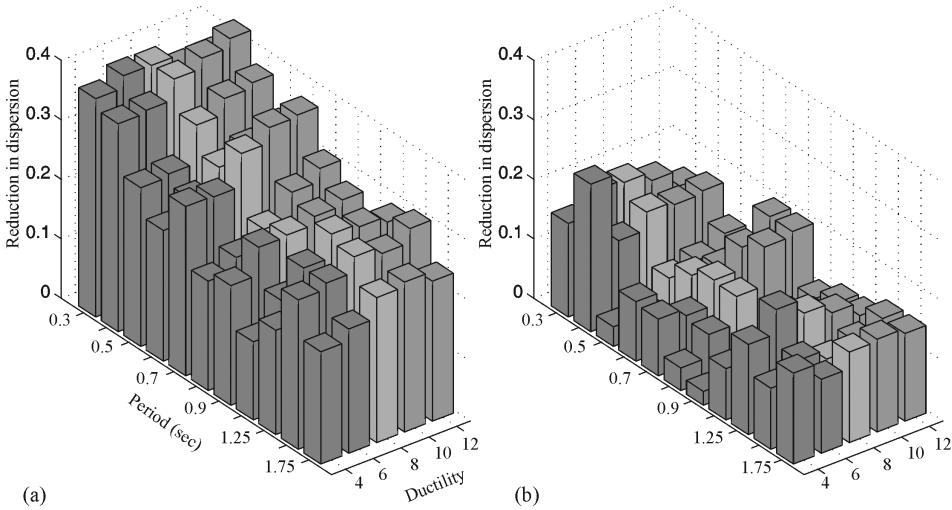


**FIGURE 9** Reduction in the dispersion of limit-state capacity due to different filtration approaches. (a)  $\eta$ -filtration and (b)  $\epsilon$ -filtration.

As a rough estimate, the dispersion of the adjusted fragility curves ( $\sigma^*$ ) was assumed to be equal to 75% of the dispersion of the general fragility curve ( $\sigma$ ) in the current study, as defined in Eq. (8):

$$\sigma^* = 0.75\sigma. \tag{8}$$

The dispersion reduction in fragility curve may not have significant effect on the loss estimation since the parametric studies by Pinto *et al.* (2004) showed that the order of magnitude of the failure probability is dictated by the hazard and not by the uncertainties/randomness in both input-output relationship and in the capacity [Pinto *et al.*, 2004].

### 4.3. Review of the Proposed Procedure

Based on the proposed simple approach for the adjustment of collapse fragility curves to different hazard levels, after analyzing the selected structure under the excitation of a general set of records, the mean and dispersion of the logarithm of the collapse capacity values can be determined. Equations (6) and (7) can be then applied to adjust the mean collapse capacity to the target hazard level. By considering dispersion equal to 75% of the general dispersion, and also assuming a normal distribution for the logarithm of the response, the target fragility curve can be obtained. Figure 10 shows flow-chart of the proposed procedure in more detail.

Details of a set of ground motion records which can be used as the general set for the collapse fragility assessment of structures are presented in Table 1. This general set, which includes 44 records (22 pairs out of the pre-used 78 records), was also used in the Applied Technology Council 63 Project (FEMA 2008) [FEMA, 2009] as part of a procedure to validate the seismic provisions for structural design. The mean values of  $\eta$  for the period range 0.1–4.0 s are shown in Fig. 11 for this general set. It is worth emphasizing that the application domain of the proposed formula is limited to period 0.3–1.75 s and the ductility value 4–12. Extension of this study to larger range of period and ductility is open for further investigations. In the following example the consistency of the proposed simple approach and the direct selection approach for the collapse capacity assessment of two complex MDOF structure has been examined.

## 5. Example: Collapse Fragility Assessment of Two MDOF Systems

The collapse capacity analysis of two MDOF test structure at different hazard levels, as performed by using the proposed simple approach, is investigated in this section, and the results are compared with the direct  $\eta$ -filtration approach.

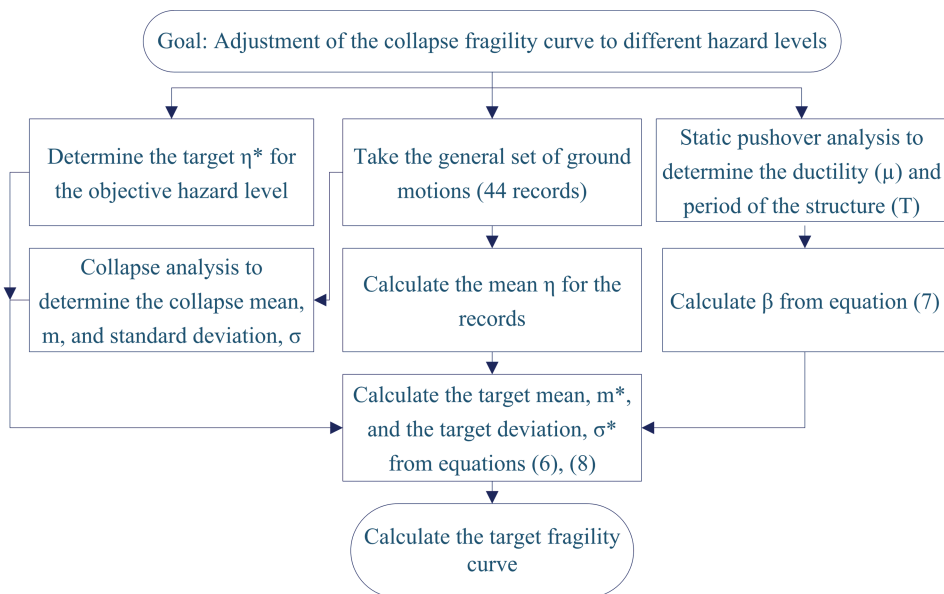


**FIGURE 10** Flowchart of the proposed approach for adjustment of the limit-state fragility curve to different hazard levels (color figure available online).

**TABLE 1** The general ground motion set used in the ATC63 project

EQ index	Mag.	Year	Event	Fault type	Station name	V <sub>s_30</sub> (m/s)	Campbell distance (km)
1	6.7	1994	Northridge	Blind thrust	Beverly Hills – 14145 Mulhol	356	17.2
2	6.7	1994	Northridge	Blind thrust	Canyon Country -W Lost Cany	309	12.4
3	7.1	1999	Duzce, Turkey	Strike-slip	Bolu	326	12.4
4	7.1	1999	Hector Mine	Strike-slip	Hector	685	11.6
5	6.5	1979	Imperial Valley	Strike-slip	Delta	275	22
6	6.5	1979	Imperial Valley	Strike-slip	El Centro Array #11	196	12.4
7	6.9	1995	Kobe, Japan	Strike-slip	Nishi-Akashi	609	25.2
8	6.9	1995	Kobe, Japan	Strike-slip	Shin-Osaka	256	28.5
9	7.5	1999	Kocaeli, Turkey	Strike-slip	Duzce	276	15.4
10	7.5	1999	Kocaeli, Turkey	Strike-slip	Arcelik	523	13.5
11	7.3	1992	Landers	Strike-slip	Yermo Fire Station	354	23.8
12	7.3	1992	Landers	Strike-slip	Coolwater	271	20
13	6.9	1989	Loma Prieta	Strike-slip	Capitola	289	35.5
14	6.9	1989	Loma Prieta	Strike-slip	Gilroy Array #3	350	12.8
15	7.4	1990	Manjil, Iran	Strike-slip	Abbar	724	13
16	6.5	1987	Superstition Hills	Strike-slip	El Centro Imp. Co. Cent	192	18.5
17	6.5	1987	Superstition Hills	Strike-slip	Poe Road (temp)	208	11.7
18	7	1992	Cape Mendocino	Thrust	Rio Dell Overpass - FF	312	14.3
19	7.6	1999	Chi-Chi, Taiwan	Thrust	CHY101	259	15.5
20	7.6	1999	Chi-Chi, Taiwan	Thrust	TCU045	705	26.8
21	6.6	1971	San Fernando	Thrust	LA - Hollywood Stor FF	316	25.9
22	6.5	1976	Friuli, Italy	Thrust	Tolmezzo	425	15.8

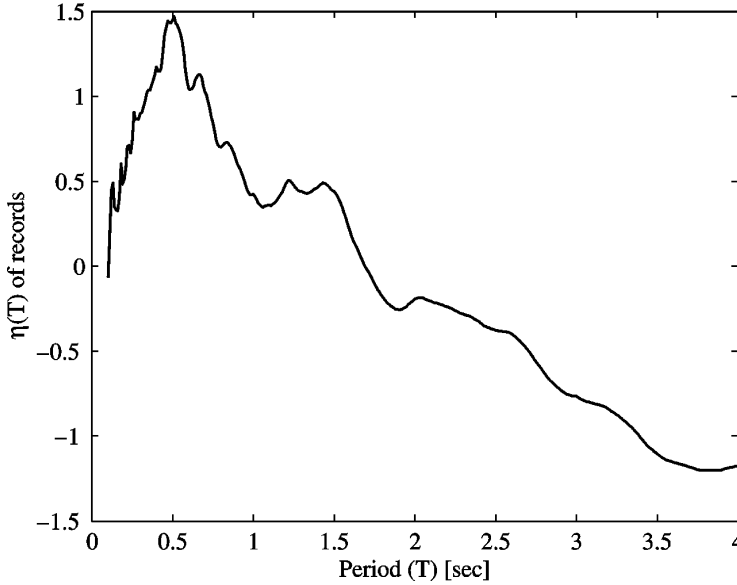


**FIGURE 11** The mean values of  $\eta$  for the general record set.

The first building had four stories with 30' bay spacing framing system, and a fundamental period ( $T_1$ ) of 0.86 s. This building has been designed for a base shear coefficient of 0.092. The details of the design have been governed according to ASCE7-05 provisions. This building has been introduced in Haselton and Deierlein [2007] with ID 1010. 295

The second reinforced concrete structure, with ID1011 [Haselton and Deierlein, 2007], had eight stories. The building is 120' x 120' in plan, uses a 3-bay perimeter frame system with 20' bay spacing, and has a fundamental period ( $T_1$ ) of 1.71 s. This reinforced concrete building has been detailed according to special moment resistant frames (SMRF) specifications in AISC7-05. The base shear coefficient of 0.05 has been considered for designing 300 of this building.

Two suitable mathematical models for these structures [Haselton and Deierlein, 2007], which were created within the OpenSees program [McKenna *et al.*, 2000], are used in this section. It was assumed that the structures are located at an idealized site, where the ground motion hazard is dominated by a single characteristic event with a return period of 200 years,  $M_w = 7.2$ ,  $R = 25$  km, and  $V_{s30} = 360$  m/s. 305

From basic probability theory, the annual frequency of exceedance ( $\nu$ ) for  $\ln S_a(T) > x$  can be written as:

$$\nu[\ln S_a(T) > x] = \nu_0 P[\ln S_a(T) > x | Mw, R], \quad (9)$$

where  $\nu_0$  is the annual frequency of the earthquake, which is in this case equal to  $\frac{1}{200}$ . At first,  $x$  is taken to be equal to be the value predicted by the attenuation relation ( $\overline{\ln S_a(T)}$ ), which corresponds to a zero epsilon value: 310

$$\nu[\ln S_a(T) > \overline{\ln S_a(T)}] = \nu_0 P[\ln S_a(T) > \overline{\ln S_a(T)} | Mw, R] = \frac{1}{200} \times 0.50 = \frac{1}{400}.$$

It is obvious that this case corresponds to the return period equal to 400 years since the exceedance of a median ground motion will occur once every 400 years because the earthquake occurs every 200 years and the median is only exceeded half of the time. Assuming a normal distribution for  $\ln S_a(T)$ , Eq. (9) can be re-written for  $\varepsilon_{Sa} = 0.20$  as:

315

$$\nu[\ln S_a(T) > \overline{\ln S_a(T)} + 0.20\sigma] = \nu_0 P[\ln S_a(T) > \overline{\ln S_a(T)} + 0.20\sigma | Mw, R] = \frac{1}{475}.$$

It is reasonable to infer that  $\varepsilon_{Sa} = 0.20$  is equivalent to an event with a return period of 475 years. Using this approach, the target epsilons for different hazard levels are given in Table 2. It is worth emphasizing that the attenuation model CB07 has been employed as a consistent model for the all considered examples.

The static pushover curves of the structures are shown in Fig. 12, showing a ductility value equal to 12 and 8.5, respectively. The ultimate ductility is fixed at a strength loss of 20%. There is an obvious negative stiffness in the pushover curve of the second structure that differs from the ideal curve fit. According to Ibarra and Krawinkler [2005], the post-yield stiffness most influences the collapse capacity of a structure. So, this parameter may also affect  $\beta$ , as well as other factors such as cyclic deterioration. This issue is open for further researches but it is neglected in the current study for the purpose of simplicity.

325

By use of the ATC63 general ground motion set (Table 1, containing 44 records), the mean collapse capacity for both of structures can be determined, and the results are adjusted to different hazard levels, as shown in Table 3. Also, for comparison purposes, Table 3 includes the collapse capacities for the different hazard levels which were evaluated based on direct  $\eta$ -filtration.

330

**TABLE 2** The target epsilon values for different hazard levels

Return Period (years)	Probability in 50 years	Target epsilon
250	18%	-0.84
475	10%	+0.20
2475	2%	+1.40

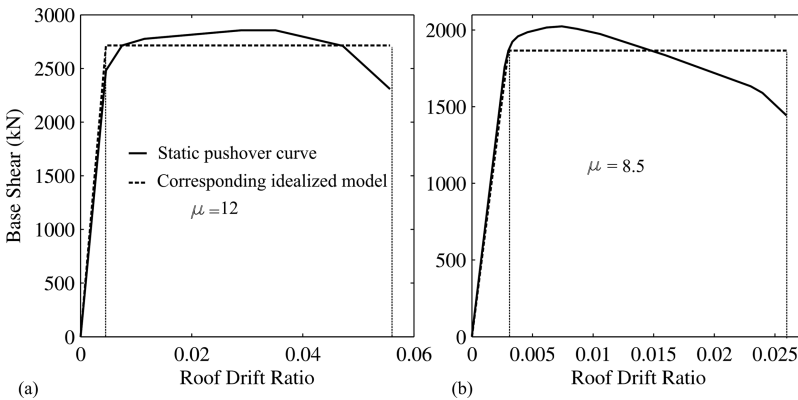


**FIGURE 12** The static pushover curve of the MDOF test structures. (a) First four-storied and (b) second eight-storied structure.

**TABLE 3** Comparison of the simple approach for the adjustment of the mean collapse capacity and the direct  $\eta$ -filtration approach

Return period (years)	The first structure collapse capacity, based on $S_a(T_1=0.86\text{sec})$ [g]			The second structure collapse capacity, based on $S_a(T_1=1.71\text{sec})$ [g]		
	Without considering $\eta$	The $\eta$ -filtration approach	The simple approach	Without considering $\eta$	The $\eta$ -filtration approach	The simple approach
250	2.63	1.89	1.90	0.72	0.57	0.59
475	2.63	2.34	2.34	0.72	0.71	0.72
2475	2.63	3.17	3.01	0.72	0.94	0.92

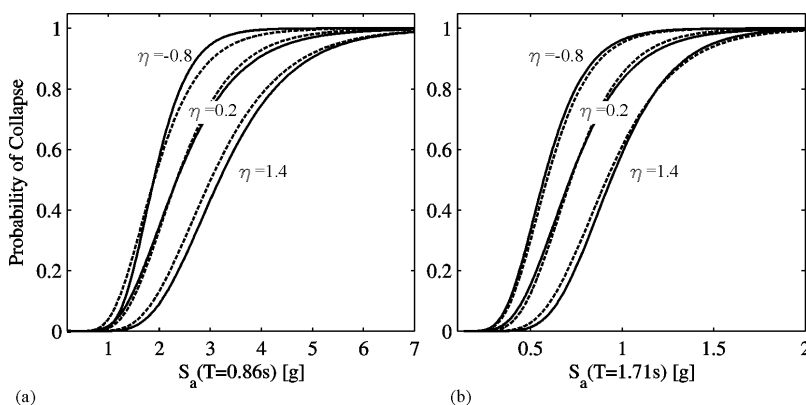


**FIGURE 13** The fragility curves for different hazard levels. (a) The first structure and (b) the second structure.

The results shown in the above table confirm the consistency of the direct approach and the proposed adjustment procedure. The resulting fragility curves for different hazard levels are shown in Fig. 13. The direct  $\eta$ -filtration approach and the simple approach show good agreement for different hazard levels, as can be seen in Fig. 13, which demonstrates that the simple approach can be used as an alternative to the direct filtration approach. 335

A simplified PEER-like approach was used here to calculate the MAF of the collapse for these two structures [Moehle and Deierlein, 2004]. That means the collapse fragility curves of the system were integrated with the site hazard curve to achieve the MAF. The calculation of the hazard curve for the assumed ideal site is a straightforward procedure. Also, the fragility curves for different hazard levels are computable through the direct  $\eta$ -filtration approach and the proposed simple approach for the adjustment of the general collapse fragility curve. In order to more investigations, the collapse fragility curves were also assessed for the direct  $\varepsilon$ -filtration approach, and for the simple approach proposed by Haselton *et al.* [2011] for the adjustment by means of  $\varepsilon$ . 340 345

Figure 14 shows different fragility curves multiplied by the assumed site hazard curve versus  $Sa(T_1)$ . Each curve in this figure corresponds to a specified fragility assessment estimation approach. As shown in this figure, the proposed simple approach shows a good agreement with the direct filtration method for both structures. This result has also been confirmed in Table 4, which states the integral values (MAFs) corresponding to each of 350

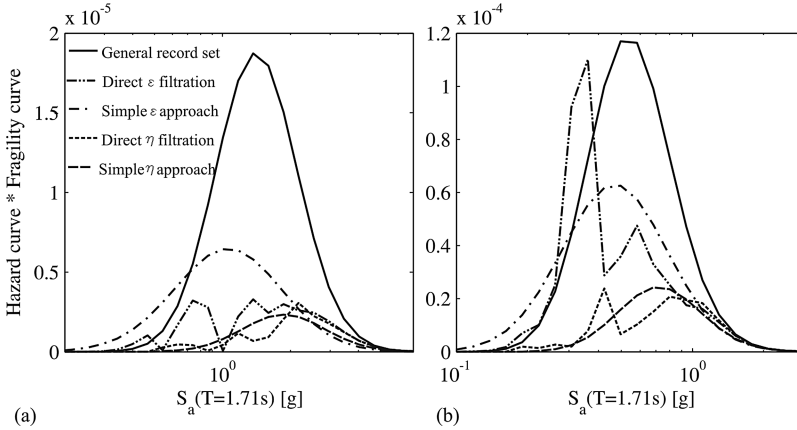


**FIGURE 14** The effect of different approaches for the consideration of spectral shape in MAF analysis. (a) First four-storied and (b) second eight-storied structure.

**TABLE 4** The MAF of collapse of the test structure according to different approaches for considering the spectral shape

Approach Name	MAF ( $\times 10^{-5}$ )	
	1st structure	2nd structure
General set without any filtration	2.8	6.7
Direct $\varepsilon$ -filtration	0.7	3.6
Simple approach considering $\varepsilon$	1.0	3.8
Direct $\eta$ -filtration	0.5	1.6
Simple approach considering $\eta$	0.4	1.7

the curves shown in Fig. 14. This table also proves the more robustness of the adjustment procedure for  $\eta$  in comparison with adjustment for  $\varepsilon$ , at least for the first structure. Anyway, by consideration of the more strength of  $\eta$  to represent the spectral shape, it can tentatively claim that the  $\eta$ -filtration approach can predict the MAF with more reliability.

## 6. Conclusions

355

By direct filtration of ground motion records based on  $\varepsilon$  or  $\eta$  at a desired level of hazard, more accurate estimates of structural response can be obtained, and potential bias in the estimated structural collapse capacity can be avoided. Since direct filtration is not a practical possibility, a simple approach has been proposed in this paper which can be used to evaluate collapse fragility curves at different hazard levels, without the need to repeat the filtration procedure. The study of the influence of  $\eta$  on structural mean collapse capacity has shown that it is controlled by both the structural period and the ductility parameters. GP was employed to obtain a simple formula for the prediction of the influence of  $\eta$  as a function of the structural characteristics. It was also shown that the average ratio of the reduction in the dispersion of the structural collapse capacity due to direct  $\eta$ -filtration is significant (25%), as opposed to  $\varepsilon$ -filtration, which provides an insignificant reduction in dispersion

360

365

(about 10%). By application of the proposed closed form formula to adjust the mean collapse capacity, and also by considering the dispersion reduction ratio, the collapse fragility curves of two four and eight-storied reinforced concrete structure were computed for different hazard levels, and compared with results obtained by using the direct  $\eta$ -filtration approach. The fragility curves resulting from both approaches showed good agreement. The computed mean annual frequencies of seismic collapse for both approaches were, also, similar. 370

It is needed to be emphasized that the application of this adjustment method is limited to periods from 0.25–3.0 s, and ductility values 4–12. 375

## Acknowledgments

The authors are very grateful to Dr. Haselton for supplying the structural models, and to Eng. A. H. Gandomi for providing valuable information about genetic programming. The authors are also very grateful to both anonymous reviewers for their valuable comments.

## References

- Abrahamson, N. A., Silva, W. J. [1997] “Empirical response spectral attenuation relations for shallow crustal earthquakes,” *Seismological Research Letters* **68**, 94–126.
- Azarbakht, A., Dolšek, M. [2011] “Progressive incremental dynamic Analysis for first-mode dominated structures,” *ASCE Journal of Structural Engineering* **137**(3), 445–455.
- Baker, J. W., Cornell, C. A. [2006] “Spectral shape, epsilon and record selection,” *Earthquake Engineering and Structural Dynamics* **34**(10), 1193–1217. 385
- Banzhaf, W., Nordin, P., Keller, R., Francone, F. [1998] *Genetic Programming – An Introduction On the Automatic Evolution of Computer Programs and its Application*, dpunkt/Morgan Kaufmann: Heidelberg/San Francisco.
- Bazzurro, P., Cornell, C. A. [1999] “On disaggregation of seismic hazard,” *Bulletin of Seismological Society of America* **89**(2), 501–520. 390
- Boore, D. M., Joyner, W. B., Fumal, T. E. [1997] “Equations for estimating horizontal response spectra and peak accelerations from western North America earthquakes: A summary of recent work,” *Seismological Research Letters* **68**(1), 128–153.
- Campbell, K. W., Bozorgnia, Y. [2007] “Campbell-Bozorgnia NGA ground motion relations for the geometric mean horizontal component of peak and spectral ground motion parameters,” *PEER Report 2007/02*. Pacific Engineering Research Center, University of California, Berkeley, California. 395
- Federal Emergency Management Agency. [2009] “Quantification of building system performance factors,” *Report No. FEMA P695*. Applied Technology Council, Redwood City, California. 400
- Haselton, C. B., Baker, J. W., Liel, A. B., Deierlein, G. G. [2011] “Accounting for ground motion spectral shape characteristics in structural collapse assessment through an adjustment for epsilon,” *ASCE Journal of Structural Engineering* **137**(3), 332–344.
- Haselton, C. B., Deierlein, G. G. [2007] “Assessing seismic collapse safety of modern reinforced concrete moment-frame buildings,” *PEER Report 2007/08*. Pacific Engineering Research Center, University of California, Berkeley, California. 405
- Ibarra, L. F., Krawinkler, H. [2005] “Global collapse of frame structures under seismic excitations,” *PEER Report 2005/06*, Pacific Engineering Research Center, University of California, Berkeley, California.
- Luco, N., Bazzurro, P. [2007] “Does amplitude scaling of ground motion records result in biased nonlinear structural drift responses?” *Earthquake Engineering and Structural Dynamics* **36**, 1813–1835. 410
- McGuire, R. K. [1995] “Probabilistic seismic hazard analysis and design earthquakes: closing the loop.” *Bulletin of the Seismological Society of America* **85**, 1257–1284.

- McKenna, F., Fenves, G. L., Jeremic, B., Scott, M. H. [2000] *Open System for Earthquake Simulations*. Available from: <http://opensees.berkeley.edu>. 415 Q4
- Moehle, J., Deierlein, G. G. [2004] "A framework methodology for performance-based earthquake engineering," *Proc. 13th World Conference on Earthquake Engineering*, Vancouver, Canada. Q5
- Mousavi, M., Ghafory-Ashtiany, M., Azarbakht, A. R. [ ] "A new indicator of elastic spectral shape for more reliable selection of ground motion records," *Earthquake Engineering and Structural Dynamics*; Published online, DOI: 10.1002/eqe.1096. 420 Q6
- PEER [ ] *Strong Motion Database*. Available from: <http://peer.Berkeley.edu/NGA>. Q7
- Pinto, P. E., Giannini, R., and Franchin, P. [2004] *Seismic Reliability Analysis of Structures*, Pavia, Italy, IUSS Press.
- Smith, G. N. [1986] *Probability and Statistics in Civil Engineering*. Collins, London. 425
- Vamvatsikos, D., Cornell, C. A. [2005] "Direct estimation of the seismic demand and capacity of multi-degree-of-freedom systems through incremental dynamic analysis of single degree of freedom approximation," *Journal of Structural Engineering* **131**(4), 589–599.
- Vamvatsikos, D., Cornell, C. A. [2002] "Incremental dynamic analysis," *Earthquake Engineering and Structural Dynamics* **31**(3), 491–514. 430
- Zareian, F., Krawinkler, H. [2007] "Assessment of probability of collapse and design for collapse safety," *Earthquake Engineering and Structural Dynamics* **36**, 1901–1914.